Efficiency roll-off suppression in organic light-emitting diodes using size-tunable bimetallic bowtie nanoantennas at high current densities

Yukun Zhao, Feng Yun, Yi Huang, Zhaoxin Wu, Yufeng Li, Bo Jiao, Lungang Feng, Sanfeng Li, Wen Ding, and Ye Zhang

Citation: Applied Physics Letters **109**, 013303 (2016); doi: 10.1063/1.4955129

View online: http://dx.doi.org/10.1063/1.4955129

View Table of Contents: http://scitation.aip.org/content/aip/journal/apl/109/1?ver=pdfcov

Published by the AIP Publishing

Efficiency roll-off suppression in organic light-emitting diodes using size-tunable bimetallic bowtie nanoantennas at high current densities

Yukun Zhao,[1,2,3] Feng Yun,[1,2,a)] Yi Huang,[3] Zhaoxin Wu,[1] Yufeng Li,[1,2] Bo Jiao,[1] Lungang Feng,[1,2] Sanfeng Li,[1] Wen Ding,[1,2] and Ye Zhang[2]
[1]*Key Laboratory of Physical Electronics and Devices of Ministry of Education and Shaanxi Provincial Key Laboratory of Photonics & Information Technology, Xi'an Jiaotong University, Xi'an, Shaanxi 710049, People's Republic of China*
[2]*Solid-State Lighting Engineering Research Center, Xi'an Jiaotong University, Xi'an, Shaanxi 710049, People's Republic of China*
[3]*Department of Electrical Engineering and Electronics, University of Liverpool, Liverpool L69 3GJ, United Kingdom*

(Received 21 March 2016; accepted 21 June 2016; published online 7 July 2016)

Size-tunable bimetallic bowtie nanoantennas have been utilized to suppress the efficiency roll-off characteristics in organic light-emitting diodes (OLEDs) using both the numerical and experimental approaches. The resonant range can be widened by the strong dual-atomic couplings in bimetallic bowtie nanoantennas. Compared with the green OLED with conventional bowtie nanoantennas at a high current density of 800 mA/cm^2, the measured efficiency roll-off ratio of the OLED with size-modulated bowtie nanoantennas is decreased from 53.2% to 41.8%, and the measured current efficiency is enhanced by 29.9%. When the size-modulated bowtie nanoantennas are utilized in blue phosphorescent OLEDs, the experimental roll-off ratio is suppressed from 43.6% to 25.9% at 250 mA/cm^2, and the measured current efficiency is also enhanced significantly. It is proposed that the efficiency roll-off suppression is mainly related to the enhanced localized surface plasmon effect, which leads to a shorter radiative lifetime. *Published by AIP Publishing.*
[http://dx.doi.org/10.1063/1.4955129]

With the advantages of easy fabrication and low cost, organic light-emitting devices (OLEDs) are bringing about revolutionary applications such as active-matrix displays and lighting sources.[1–4] Yet, a crucial issue hindering the commercialization of OLEDs is related to the efficiency roll-off characteristics, which means that OLEDs deliver a high efficiency only at a low current and a low brightness, not at the higher current and brightness.[5–9] As the localized surface plasmon (LSP) effect of metallic nanoparticles (NPs) can induce large local electromagnetic field enhancements, it was widely considered as an effective route to improve the performance of optoelectronic devices, including OLEDs and organic photovoltaic (OPV) devices.[10–15] It is also reported that the degree of peak energy matching between the LSP resonant energy and the energy of light determines the LSP enhancement factor,[7,10] which means that the closer these two energies are, the more the resulting performances of optoelectronic devices will be enhanced.[10] Some research works have been done to adjust the LSP resonant energy with the emitted photon energy, including tuning the size and type of the metallic NPs.[7,13,16] However, it is still a challenge to achieve a wide LSP resonance in a controlled fashion, especially in the mass production.[7,16,17] Furthermore, it has been reported that strong resonances can be achieved in bimetallic materials, which can be used for tuning LSP resonance.[18–23] To date, very few papers have been published in this area about utilizing bimetallic alloys to suppress efficiency roll-off characteristics in OLEDs.

[a)]Author to whom correspondence should be addressed. Electronic mail: fyun2010@mail.xjtu.edu.cn.

In addition, compared with chemically synthesized metallic NPs, metallic bowtie nanoantennas fabricated by e-beam evaporation have more uniform distribution and size.[11,13,14] Metallic bowtie nanoantennas can also highly enhance the optical field on the metallic surface and in between the two bowties, showing great potential for increasing the radiative emission rate as well as the intrinsic quantum efficiency.[24] In our previous work, we discussed a method of fabricating monometallic bowtie nanoantennas and its enhancement in OLEDs.[11] However, so far, the utilization of bimetallic bowtie nanoantennas is yet to be implemented to suppress efficiency roll-off characteristics of OLEDs, not to mention modulating the bowtie size. In this paper, we modulate the size of bimetallic bowtie nanoantennas to achieve the superior effect in suppressing the efficiency roll-off characteristics of OLEDs.

Fig. 1 is a schematic of the fabrication procedure for making samples with size-tunable bowtie nanoantennas. First, as shown in Fig. 1(a), a hexagonally ordered monolayer template of 200-nm-diameter polystyrene (PS) spheres was coated onto a cleaned ITO layer by the self-assembly method.[11] Second, the annealing process was performed to modulate the size of PS spheres [Fig. 1(b)]. Samples were mounted on a heating plate with the temperature of ~390 K. After that, a 15-nm-thick bimetallic film (Au/Sn alloys) was deposited on the ITO layer by electron beam evaporation [Fig. 1(c)]. Then, the chloroform solution was utilized to remove the PS spheres to obtain bowtie nanoantennas on the ITO layer [Fig. 1(d)]. For OLED fabrication [Fig. 1(e)], a 25-nm-thick 4,4′,4″-tris [2-naphthyl(phenyl)amino] triphenylamine (2T-NATA) film was spin-coated onto the ITO layer, which was used as the hole injection layer and spacer.

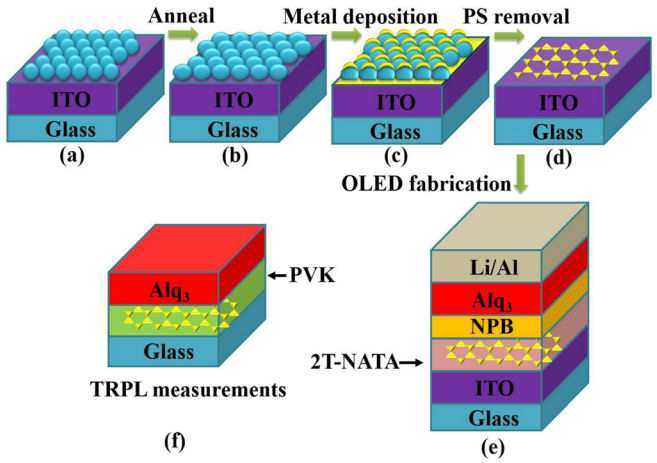

FIG. 1. Schematic of the processes for fabricating bowtie nanoantennas. (a) PS spheres self-assembled on ITO layer. (b) PS annealing process. (c) Metal film deposited on the ITO layer. (d) PS sphere removal. (e) OLED structure with bowtie nanoantennas. (f) Sample for TRPL measurements.

A 5-nm-thick *N*,*N*′-di-[(1-naphthalenyl)-*N*,*N*′-diphenyl]-(1,1′-biphenyl)-4,4′-diamine (NPB) film and a 60-nm-thick tris(8-quinolinolato)aluminum (Alq_3) film were successively deposited on the 2T-NATA film, which acted as the hole transporting layer and emission/electron-transporting layer, respectively. After that, a 100-nm-thick LiF/Al film was deposited as the cathode in the OLED device with an area of $\sim 3 \times 3\,mm^2$. To avoid unwanted light scattering by the LiF/Al film in OLED devices [Fig. 1(e)], the samples shown in Fig. 1(f) were tailored to replace the actual OLED devices to be used for time-resolved photoluminescence (TRPL) measurements. As illustrated in Fig. 1(f), after the removal of PS spheres, a 30-nm-thick polyvinyl carbazole (PVK) film was spin-coated onto the ITO layer, and subsequently covered with a 60-nm-thick Alq_3 film as the emission layer. As shown in Figs. 1(e) and 1(f), the distances between the upper surface of bowtie nanoantennas and the lower surface of the emission layer (Alq_3) remained constant ($\sim$15 nm). In the annealing process of Fig. 1(b), the diameter of the PS beads was continuously increased while the center of the PS spheres remained fixed. The heating durations of samples A and B were 0 s and $\sim$5 s, respectively. The mass fraction of Au in the Au/Sn alloys is $\sim$80%.

Scanning electron microscopy (SEM) was used to characterize the quality of PS and bowtie nanoantennas, and the atomic force microscopy (AFM) was used to characterize the surface morphology of the films. Fig. 2 is a collection of the surface micrographs by SEM and AFM. It can be clearly seen from Figs. 2(a) and 2(c) that, with the increase in heating duration from 0 s to $\sim$5 s, the mask apertures surrounded by three adjacent PS beads shrink gradually. The length of each side of bowtie nanoantennas decreases from $\sim$80 nm to $\sim$65 nm when the PS mask annealed from 0 s to $\sim$5 s, respectively, which were scanned on silicon wafers. After spin-coating a 25-nm-thick 2T-NATA film, a flat surface was achieved, resulting in that the underlying bowtie nanoantennas have little influence on the electrical properties of OLED devices.

Three-dimensional (3D) finite-difference time-domain (FDTD) models using commercial software FDTD Solutions were utilized to investigate the optical properties of bowtie nanoantennas. The refractive index of the background is set to be 1.0. The plan waves were used as the lighting source to excite transverse-electric (TE) modes. The proportion of mass fraction of the bimetallic alloys (Au:Sn) is 80:20, and the relative atomic mass of Au and Sn is 197.0 and 118.7, respectively. Therefore, the proportion of atomic quantity in the Au/Sn alloys is $N_{Au}{:}N_{Sn} = 80/197.0{:}20/118.7 = 9.6{:}4$. As the packing form of Au crystal is face-centered cubic (FCC) shown in Fig. 3(a), to simplify the simulations, the dual-atomic simulation model is set to such that 2 Au atoms in the face center are replaced by 2 Sn atoms.[21,22] Consequently, the proportion of atomic quantity in the unit cell of the dual-atomic model is $N'_{Au}{:}N'_{Sn} = (8 \times 1/8 + 4 \times 1/2){:}2 \times 1/2 = 3{:}1$, which is similar to that of Au/Sn alloys.

Fig. 3(b) shows that the strong dual-atomic couplings exist between the two different atoms, which could lead to a stronger LSP effect.[18,21–23] As shown in Fig. 3(c), compared with those in Refs. 1, 6, and 11–13, a much widened peak resonant range of region A ($\sim$560 nm to $\sim$780 nm) is obtained, which could result from that strong dual-atomic couplings adjust the momentum of LSPs to couple with radiated

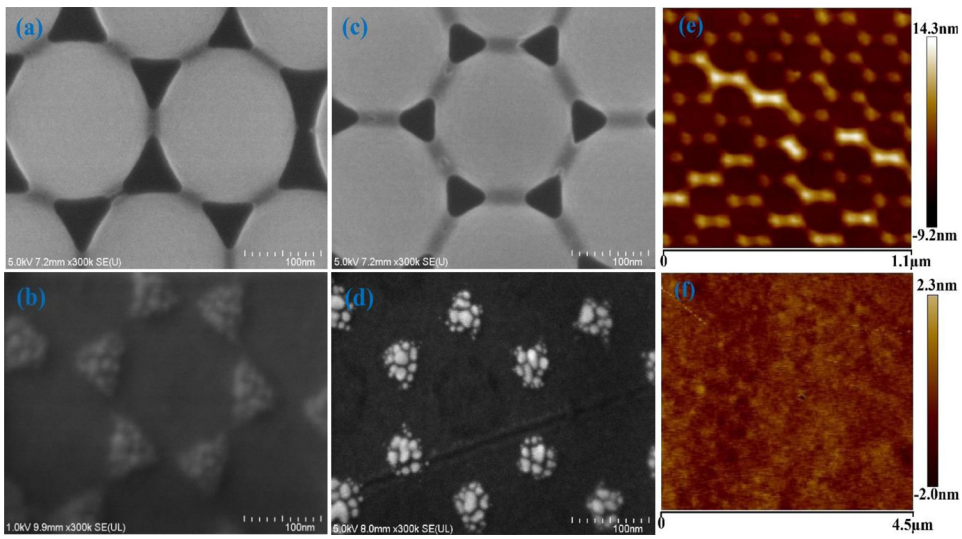

FIG. 2. Experimental top-view SEM images of PS spheres annealed (a) 0 s and (c) $\sim$5 s. $\sim$30°-tilted SEM images of bowtie nanoantennas on the substrates annealed (b) 0 s and (d) $\sim$5 s. Experimental AFM images of the sample with bowtie nanoantennas (e) before and (f) after spin coating a 2T-NATA film.

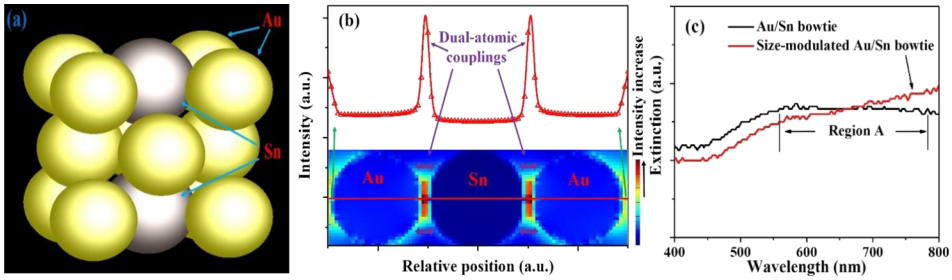

FIG. 3. (a) Dual-atomic simulation model. (b) Simulated electrical field intensity of the red line (monitoring position) in the dual-atomic model, incorporated image is the simulated electrical field distribution of dual-atomic couplings at the wavelength of 520 nm. (c) Measured extinction spectra.

lights.[25–27] The widened peak resonant range has a better chance to match the LSP resonant energy and the emitted photon energy. When the size of bimetallic bowtie nanoantennas is modulated by ~5 s annealing process, the peak resonant range is not sensitive to shift, which is different from the monometallic bowtie nanoantennas.[28] In addition, according to the Mie theory,[29–31] when the size of nanostructures reduced, the absorption proportion (Q_A/Q_E) in the extinction (Q_E) could increase.[31] That means that more extinction intensities are able to be absorbed by the size-modulated bowtie nanoantennas, which could lead to the higher LSP effect.

To further verify the LSP effect, TRPL spectra were measured and illustrated in Fig. 4. Room-temperature TRPL measurements were done using a fluorescence lifetime spectrometer excited by a plused nitrogen 337 nm laser. A spectrometer and a charge-coupled device (CCD) were also used to collect the luminescence. The TRPL spectra and lifetime data are fitted and calculated as[11,32]

$$f(t) = \mathrm{A} \cdot \exp\left(-\frac{t}{\tau}\right), \tag{1}$$

$$\tau_r = \frac{2\tau_{initial}\tau_{final}}{\tau_{final} - \tau_{initial}}, \tag{2}$$

where A and τ represent the constant and lifetime, respectively. The $\tau_{initial}$, τ_{final}, and τ_r are the lifetimes at the initial stage, final stage, and the radiative lifetime, respectively. $f(t)$ represents the normalized intensity in Fig. 4. When calculating the carrier lifetimes, we adopt the standards: (a) $f(t) > 0.5$ for the initial stage, (b) $f(t) < 0.5$ for the final stage. On each stage, the data of $\tau_{initial}$, τ_{final} are calculated using Eq. (1). It has been reported that the coupling between LSPs and radiated light is faster than spontaneous recombination of excitons, and the exciton lifetime in LSP-enhanced samples should be decreased.[14] As shown in Fig. 4, the experimental τ_r at 520 nm decreases from 27.4 ns (sample A) to 19.1 ns (sample B), indicating that a stronger LSP effect could be observed between the size-modulated bowtie nanoantennas and the emission layer (Alq_3).

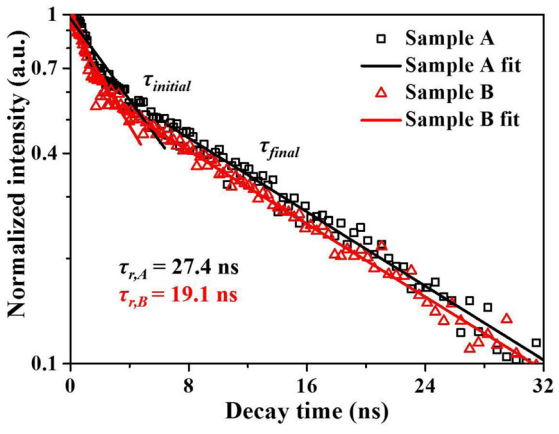

FIG. 4. Experimental TRPL spectra and fitting lines of samples A and B at the wavelength of 520 nm.

To make the OLED measurements more accurate, two samples were randomly selected and measured for both samples A and B. The average data of the measured I-V-luminance characteristics, current efficiency, and efficiency roll-off ratio of samples A and B are summarized in Fig. 5. The current density–brightness–voltage (J–B–V) characteristics were measured using a Keithley 2602 Source Meter. The efficiency roll-off ratio (Q) is defined and calculated as[11]

$$Q = \frac{\eta_{\max} - \eta}{\eta_{\max}}, \tag{3}$$

where $\eta_{\max}$ and η are the maximum current efficiency and the current efficiency at an arbitrary current density, respectively. For instance, as the $\eta_{\max}$ is 3.99 cd/A and η is 2.45 cd/A at 596 mA/cm^2, the efficiency roll-off ratio (Q) of sample A is (3.99–2.45)/3.99 ≈ 38.6% at 596 mA/cm^2. From Fig. 5(a), it is clear that samples A and B have almost identical electrical behavior. Compared to that of Au bowtie nanoantennas in Ref. 11, the integration of Sn atoms could deteriorate the I-V characteristic, which limits the efficiency improvement. However, in Fig. 5(b), compared with sample A at a high current density of 800 mA/cm^2, the measured current efficiency of sample B with the size-modulated Au/Sn bowtie nanoantennas is enhanced by 29.9%, increasing from 1.87 cd/A to 2.43 cd/A. The luminance spectra in Fig. 5(a) also show a significant intensity enhancement. The experimental roll-off ratio is suppressed from 53.2% (sample A) to 41.8% (sample B) at 800 mA/cm^2. In our previous work,[11] the efficiency roll-off suppression for the sample with bowtie nanoantennas was mainly attributed to the LSP effect. The enhanced efficiency roll-off suppression of sample B with the size-modulated bowtie nanoantennas associates with the enhanced LSP effect, supported by the shorter radiative lifetime as observed in Fig. 4.

To further demonstrate the efficiency roll-off suppression, we fabricated the size-tunable bowtie nanoantennas into blue phosphorescent OLED devices, which still remain a technical challenge of efficiency roll-off.[33,34] As silver (Ag) is in general the best material for the blue spectral region,[7] the metal in the deposition process of Fig. 1(c) is Ag. 500-nm-diameter PS spheres were utilized as the

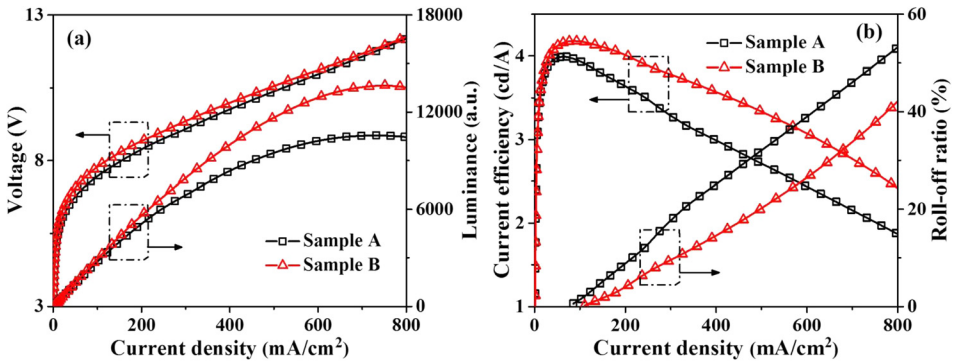

FIG. 5. Experimental spectra of (a) I-V–luminance characteristics, and (b) current efficiency and efficiency roll-off ratio of samples A and B.

monolayer template. The structure of the phosphorescent OLEDs is 2T-NATA (20 nm)/TAPC (15 nm)/mCP:FIrpic (15 nm)/TPBi (40 nm)/LiF (1 nm)/Al (100 nm) (Fig. 6). The materials of TAPC, mCP, and TPBi are 1,1-bis[(di-4-tolylamino)phenyl]cyclohexane (hole transport layer), *N*,*N*′-dicarbazolyl-3,5-benzene (host material), and 2,2′,2″-(1,3,5-benzinetriyl)-tris(1-phenyl-1-H-benzimidazole) (electron transport layer), respectively. The blue phosphorescent doping concentration of iridium (III) bis[(4,6-difluorophenyl)-pyridinato-N,C^2]-picolinate (FIrpic) is ∼10%. The fabrication processes of samples C and D are the same, except that the heating durations of samples C and D in the annealing process [Fig. 1(b)] were 0 s and ∼5 s, respectively.

As clearly shown in Fig. 6, compared with sample C at a high current density of 250 mA/cm^2, the measured current efficiency of sample D with size-modulated bowtie nanoantennas is enhanced by 32.7%, increasing from 10.1 cd/A to 13.4 cd/A. The experimental roll-off ratio is suppressed from 43.6% (sample C) to 25.9% (sample D) at 250 mA/cm^2.

In conclusion, we have demonstrated the utilization of size-tunable bimetallic bowtie nanoantennas in OLEDs to suppress efficiency roll-off characteristics. Incorporating bimetallic bowtie nanoantennas could be a promising way to improve the insufficient couplings by widening the resonant range. Compared with the green OLED with conventional bowtie nanoantennas at a high current density of 800 mA/cm^2, the measured efficiency roll-off ratio of the OLED with size-modulated bowtie nanoantennas decreases from 53.2% to 41.8%, and the measured current efficiency is enhanced by 29.9%. The significant efficiency enhancement and marked roll-off suppression can also be achieved when the size-modulated bowtie nanoantennas utilized in blue phosphorescent OLEDs. This efficiency roll-off suppression is mainly attributed to the enhanced LSP effect of the size-modulated bowtie nanoantennas, leading to the shorter radiative lifetime. Finally, the ability to fabricate size-tunable bimetallic bowtie nanoantennas by itself is of great potential significance to a wide range of optoelectronic devices.

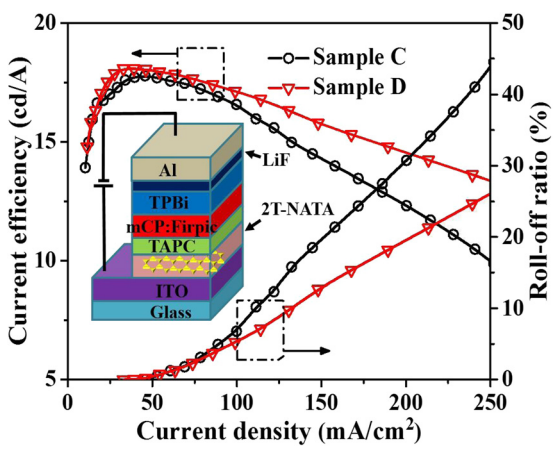

FIG. 6. Experimental current efficiency and efficiency roll-off ratio of samples C and D. The inset image is the schematic of phosphorescent OLED structure.

This project was supported by the National High Technology Research and Development Program (863) of China (Project No. 2014AA032608), Key Research Program of China (2016YFB0400702), China Scholarship Council (CSC No. 201506280046), and the Fundamental Research Funds for the Central Universities. We would also like to thank Dr. Yue Yu for his help on the fabrication of blue phosphorescent OLED devices.

[1]Y. H. Lee, D. H. Kim, K. H. Yoo, and T. W. Kim, Appl. Phys. Lett. **105**, 183303 (2014).
[2]Y. M. Yin, X. M. Wen, J. Yu, L. T. Zhang, and W. F. Xie, IEEE Photonics Technol. Lett. **25**, 2205 (2013).
[3]S. Reineke, F. Lindner, G. Schwartz, N. Seidler, K. Walzer, B. Lüssem, and K. Leo, Nature **459**, 234 (2009).
[4]Y. J. Doh, J. S. Park, W. S. Jeon, R. Pode, and J. H. Kwon, Org. Electron. **13**, 586 (2012).
[5]K. Hayashi, H. Nakanotani, M. Inoue, K. Yoshida, O. Mikhnenko, T. Q. Nguyen, and C. Adachi, Appl. Phys. Lett. **106**, 093301 (2015).
[6]W. Y. Ji, L. T. Zhang, and W. F. Xie, Opt. Lett. **37**, 2019 (2012).
[7]I. H. Lee, L. W. Jang, and A. Y. Polyakov, Nano Energy **13**, 140 (2015).
[8]N. Sun, Y. Zhao, F. Zhao, Y. Chen, D. Yang, J. Chen, and D. Ma, Appl. Phys. Lett. **105**, 013303 (2014).
[9]C. Murawski, P. Liehm, K. Leo, and M. C. Gather, Adv. Funct. Mater. **24**, 1117 (2014).
[10]X. T. Liu, D. B. Li, X. J. Sun, Z. M. Li, H. Song, H. Jiang, and Y. R. Chen, Sci. Rep. **5**, 12555 (2015).
[11]Y. K. Zhao, F. Yun, Z. X. Wu, Y. F. Li, B. Jiao, Y. Y. Huang, S. F. Li, L. G. Feng, M. F. Guo, W. Ding, Y. Zhang, and J. Dou, Appl. Phys. Express **9**, 022101 (2016).
[12]W. Y. Ji, P. T. Jing, and J. L. Zhao, J. Mater. Chem. C **1**, 470 (2013).
[13]A. Fujiki, T. Uemura, N. Zettsu, M. Akai-Kasaya, A. Saito, and Y. Kuwahara, Appl. Phys. Lett. **96**, 043307 (2010).
[14]Y. Xiao, J. P. Yang, P. P. Cheng, J. J. Zhu, Z. Q. Xu, Y. H. Deng, S. T. Lee, Y. Q. Li, and J. X. Tang, Appl. Phys. Lett. **100**, 013308 (2012).
[15]E. Stratakis and E. Kymakis, Mater. Today **16**, 133 (2013).
[16]Y. C. Chen, C. Y. Gao, K. L. Chen, and C. J. Huang, Appl. Surf. Sci. **295**, 266 (2014).
[17]R. J. Peláez, C. E. Rodríguez, and C. N. Afonso, Nanotechnology **27**, 105301 (2016).

[18]D. R. Jung, J. Kim, S. Nam, C. Nahm, H. Choi, J. I. Kim, J. Lee, C. Kim, and B. Park, Appl. Phys. Lett. **99**, 041906 (2011).
[19]B. J. Roxworthy and K. C. Toussaint Jr., Sci. Rep. **2**, 660 (2012).
[20]A. Malasi, J. Ge, C. Carr, H. Garcia, G. Duscher, and R. Kalyanaraman, Part. Part. Syst. Charact. **32**, 970 (2015).
[21]S. Li, L. Chen, T. Zhai, Y. Wang, L. Wang, and X. Zhang, Opt. Eng. **54**, 067110 (2015).
[22]Z. M. Adriana, M. Martyna, D. Magdalena, and G. Ewelina, Adv. Colloid Interface Sci. **229**, 80 (2016).
[23]C. H. Liu, M. H. Hong, H. W. Cheung, F. Zhang, Z. Q. Huang, L. S. Tan, and T. S. A. Hor, Opt. Express **16**, 10701 (2008).
[24]A. Kinkhabwala, Z. Yu, S. Fan, Y. Avlasevich, K. Müllen, and W. E. Moerner, Nat. Photonics **3**, 654 (2009).
[25]M. K. Kwon, J. Y. Kim, B. H. Kim, I. K. Park, C. Y. Cho, C. C. Byeon, and S. J. Park, Adv. Mater. **20**, 1253 (2008).
[26]K. Okamoto, I. Niki, A. Scherer, Y. Narukawa, T. Mukai, and Y. Kawakami, Appl. Phys. Lett. **87**, 071102 (2005).
[27]Z. Q. Liang, J. Sun, Y. Y. Jiang, L. Jiang, and X. D. Chen, Plasmonics **9**, 859 (2014).
[28]A. Taguchi, Y. Saito, K. Watanabe, S. Yijian, and S. Kawata, Appl. Phys. Lett. **101**, 081110 (2012).
[29]A. L. Aden and M. Kerker, J. Appl. Phys. **22**, 1242 (1951).
[30]M. J. Pilat, Appl. Opt. **6**, 1555 (1967).
[31]S. F. Li, Master thesis, Xi'an Jiaotong University, China, 2015.
[32]Q. Li, S. Wang, Z. N. Gong, F. Yun, Y. Zhang, and W. Ding, Optik **127**, 1809 (2016).
[33]S. I. Yoo, J. A. Yoon, N. H. Kim, J. W. Kim, J. S. Kang, C. B. Moon, and W. Y. Kim, J. Lumin. **160**, 346 (2015).
[34]J. S. Kang, S. I. Yoo, J. W. Kim, G. J. Yoon, S. Yi, and W. Y. Kim, Opt. Mater. **52**, 181 (2016).